J|A|C|S
ARTICLES
Published on Web 06/27/2006

Combined Magnetic and Single-Crystal X-ray Structural Study of the Linear Chain Antiferromagnet $[(CH_3)_4N][MnCl_3]$ under Varying Pressure

Somchai Tancharakorn,[†,‡] Francesca P. A. Fabbiani,[†,§] David R. Allan,[†,§] Konstantin V. Kamenev,*[,†,‡] and Neil Robertson*[,†,§]

Contribution from the Centre for Science at Extreme Conditions, School of Engineering and Electronics, School of Chemistry, University of Edinburgh, King's Buildings, Mayfield Road, Edinburgh EH9 3JZ, United Kingdom

Received March 21, 2006; E-mail: Neil.Robertson@ed.ac.uk

Abstract: The magnetic susceptibility and single-crystal X-ray structure of the one-dimensional Heisenberg antiferromagnetic chain tetramethylammonium manganese trichloride (TMMC) have been studied under pressure as a facile route to develop structure−property relationships. The X-ray structure of TMMC was determined at 0, 2.1, 3.8, 6.8, 12.2, and 17.0 kbar using diamond−anvil cell techniques and synchrotron radiation. The space group is confirmed to be $P6_3/m$ up to 17 kbar, and structural refinement shows that the Mn−Mn separations between and along the chains change by about 3.4 and 2.5%, respectively, over 17 kbar. A structural transition from hexagonal to monoclinic symmetry possibly occurs at 17 kbar, associated with a loss of crystal quality. Variable-temperature magnetic susceptibility data were taken at 0, 0.3, 1.5, 2.9, 4.0, 5.2, and 6.5 kbar and show that the intrachain coupling constant changes from −6.85 to −7.81 K over this range. The interchain coupling constant of −0.54 K can also be extracted from the Fisher model modified for interacting chains. The pressure−temperature diagram shows the slope of the intrachain antiferromagnetic coupling with pressure, $\Delta T_{IAF}/\Delta P$, changes from 0.5 to 1.6 K/kbar at 2 kbar where the structure changes from $P2_1/a$ to $P2_1/m$. Comparison of the magnetic and structural data are consistent with the power−law relationship developed by Bloch where $J \propto r^{-n}$, r = Mn···Mn separation and $n \approx 10$.

Introduction

One of the central elements in the study of magnetic materials is the development of structure−property relationships.[1] This can take the form of an empirical relationship that enables the prediction of magnetic properties within a series of materials or can involve a deeper fundamental understanding of the origin of magnetic interactions and bulk magnetic behavior. These are typified by examples such as the well-known Goodenough and Kanamori rules that describe the angle-dependence of superexchange in bridged transition metal species,[2,3] and such considerations have led to both an empirical correlation and also an understanding of the orbital origin of the relationship in, for example, hydroxo-bridged and related Cu(II) dimers.[4−7] Other examples exist such as the structural dependence of superexchange in Fe(III)···O···Fe(III) systems,[8] bridged Cr(III) dimers,[9] azide-bridged Mn(II) species,[1] Ni-cubanes,[10] and linear fluoride-bridged Mn(II), Co(II), and Ni(II) systems.[11] Inevitably, the development of robust and reliable structure−property relationships involves the acquisition of a large body of empirical data from variable-temperature magnetic susceptibility studies alongside single-crystal X-ray diffraction of a large number of examples, all of which must be individually synthesized, characterized, and analyzed. The large amount of work this entails serves as a barrier to development of this field as evidenced by many examples where insufficient related complexes are available to develop a reliable correlation.[5]

In this work, we explore a novel approach to this topic that involves the use of high pressure to steadily alter both the structure and magnetic properties of a single material such that relationships between the two can be sought. The method allows the rapid and facile acquisition of a significant body of experimental data, and this work details our first results using this approach.

The effects of pressure on magnetic properties of materials was explored by Bloch[12] for the case of simple insulating magnetic materials, leading to an empirical relationship between

[†] Centre for Science at Extreme Conditions.
[‡] School of Engineering and Electronics.
[§] School of Chemistry.

(1) Karmakar, T. K.; Ghosh, B. K.; Usman, A.; Fun, H.-K.; Riviere, E.; Mallah, T.; Aromi, G.; Chandra, S. K. *Inorg. Chem.*, **2005**, *44*, 2391.
(2) Goodenough, J. B. *J. Phys. Chem. Solids* **1958**, *6*, 287.
(3) Kanamori, J. *J. Phys. Chem. Solids* **1959**, *10*, 87.
(4) Crawford, V. H.; Richardson, H. W.; Wasson, J. R.; Hodgson, D. J.; Hatfield, W. E. *Inorg. Chem.* **1976**, *15*, 2107.
(5) Hodgson, D. J. *Prog. Inorg. Chem.* **1975**, *19*, 173.
(6) Thompson, L. K.; Mandal, S. K.; Tandon, S. S.; Bridson, J. N.; Park, M. K. *Inorg. Chem.* **1996**, *35*, 3117.
(7) Rodriguez-Fortea, A.; Ruiz, E.; Alvarez, S.; Alemany, P. *Dalton Trans.* **2005**, 2624.
(8) Gorum, S. M.; Lippard, S. J. *Inorg. Chem.* **1991**, *30*, 162.
(9) Castell, O.; Caballol, R. *Inorg. Chem.* **1999**, *38*, 668.
(10) Clemente-Juan, J. M.; Chansou, B.; Donnadieu, B.; Tuchagues, J.-P. *Inorg. Chem.* **2000**, *39*, 5515.
(11) De Jongh, L. J.; Block, R. *Physica B* **1975**, *79*, 568.
(12) Bloch, D. *J. Phys. Chem. Solids* **1966**, *27*, 881.

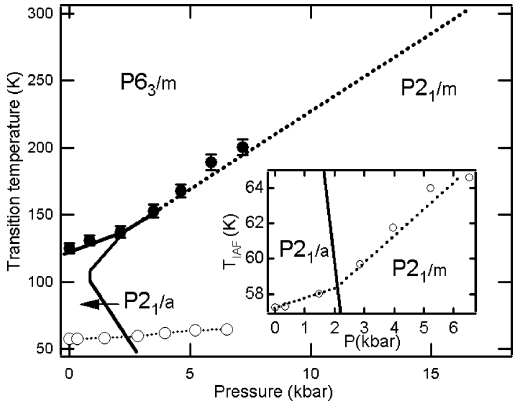

Figure 1. Pressure−temperature phase diagram of TMMC in the region around 50−300 K and 0−18 kbar. The solid line is taken from the work of Peercy,[22] and all data points (filled and empty circles) are from the magnetic studies in this work (see below). (Inset) Expansion of the low T and P region and the dT_{IAF}/dP (dotted line) changes from 0.5 K/kbar to 1.6 K/kbar at 2 kbar crossing the (solid) line of the structural phase transition.

exchange coupling and distance of the form $J \propto r^{-n}$ where $n \approx 10$ with later work indicating $n \approx 12$,[11] and this has been shown to be consistent with the exponential relationship expected through overlap of adjacent magnetic orbitals.[11,13] Clearly, this relationship cannot apply in a general sense to all exchange-coupling geometries, where factors such as angular dependence play a crucial role,[2,3] and little further experimental work has been carried out to compare this relationship to systems with different structural motifs.

We chose tetramethylammonium manganese trichloride ($[(CH_3)_4N][MnCl_3]$, known as TMMC), as the model system for study. It is one of a large series of ABX_3 system, where A is a monocation, B is the magnetic ion, and X is a halogen.[14] The system is highly one-dimensional with a Heisenberg antiferromagnetic chain of S = 5/2 Mn(II) ions and is well-known as a model magnetic material. The lack of complications from single-ion effects or multidimensional behavior suggested this as an excellent model system for our studies, with the magnetic properties in the temperature range of study effectively dependent on only one parameter, the intrachain exchange coupling constant.

The ambient pressure structure of TMMC is hexagonal and consists of infinite chains of spin-$^5/_2$ manganese atoms along the c axis bridged by three chloride ligands. The manganese chains are thoroughly separated by the tetramethylammonium counterions leading to ideal one-dimensional antiferromagnetic chains. Separation of the chains by inclusion of the organic counterions leads, through changes in the orientation and ordering of these,[15−19] to structural phase transitions that have been studied at ambient pressure and under pressure for many years (Figure 1).[20,21,22] At ambient pressure and 126 K, TMMC

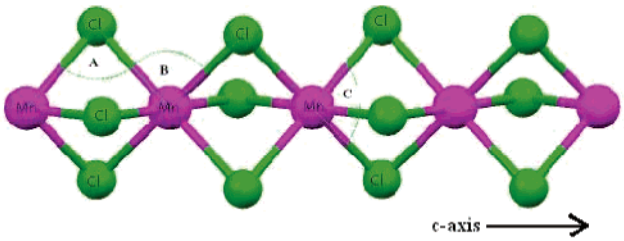

Figure 2. Infinite chain of Mn atoms along the c axis bridged by three chlorine atoms. Angles A, B, and C are defined as shown.

exhibits an order−disorder structural phase transition from hexagonal ($P6_3/m$ and $Z = 2$) to monoclinic ($P2_1/a$ and $Z = 4$), and an additional monoclininc phase ($P2_1/m$ and $Z = 2$)[21,22] is observed under pressure as shown by dielectric constant measurements (Figure 1). Although this may lead to complications in analysis of the variable-temperature magnetic properties, all of the known phases retain analogous well-separated Mn(II) chains running along the c axis (Figure 2). It will be interesting to observe the extent to which the structural phase transitions influence the magnetic behavior of the system and whether this limits the choice of model systems for future variable-pressure−temperature studies.

Experimental Section

TMMC crystals were grown at room temperature through evaporation. Pink hexagonal rods longer than 1 cm were obtained from a solution of 10% HCl, tetramethylammonium chloride, and manganese dichloride over one week. A crystal of about 2.5 mm in length was selected for the magnetic measurement.

Magnetic Susceptibility Measurements under Pressure. A piston−cylinder type pressure cell was used for measurement of the magnetic susceptibility. The cell has been specially designed for use in a commercial superconducting quantum interference device magnetometer (Quantum Design MPMS), SQUID,[23] and is made of copper−beryllium alloy, which gives a very weak signal. It has been calibrated by studying the superconducting temperature of lead as a function of the diameter of the pressure cell, such that lead is not required to be present during the sample runs, allowing us to conduct the experiment with a very low background at low temperature. The pressure inside the cell can be calculated by $\Delta P/\Delta d = 0.62$ kbar/μm, where ΔP is the pressure difference and Δd is the diameter difference of the outer cell. Owing to the solidification of the pressure medium, the pressure at low temperature is lower than at room temperature, and compensation for this has allowed the pressure at different temperatures to be determined reliably.[24]

The magnetic susceptibility of TMMC was measured in the temperature range of 2−300 K and pressure from 0 to 6.5 kbar. The properties of the crystal were first confirmed by measuring the magnetic susceptibility parallel and perpendicular to the c axis in a gelatin capsule showing good agreement with literature data.[25] The crystal was loaded in the pressure cell surrounded by Daphne 7373 oil as the pressure transmitting medium,[26] and the measurements were carried out at a series of pressures.

High-Pressure X-ray Diffraction. A sample crystal was loaded into a Merrill−Bassett diamond−anvil cell,[27] equipped with 600 μm culet diamonds and a tungsten gasket. A small chip of ruby was placed beside

(13) Bramwell, S. T. *J. Phys:. Condens. Matter* **1990**, *2*, 7527.
(14) De Jongh, L. J.; Miedema, A. R. *Adv. Phys.* **1974**, *23*, 1.
(15) Morosin, B.; Graeber, E. J. *Acta Crystallogr.* **1967**, *23*, 766.
(16) Jewess, M. *Acta Crystallogr., Sect. B: Struct. Sci.* **1982**, *38*, 1418.
(17) Guillaume, F.; Couzi, M.; Bée, M. *Physica B* **1992**, *180&181*, 714.
(18) Rodriguez, V.; Guillaume, F.; Couzi, M. *J. Phys. Chem.* **1996**, *100*, 14109.
(19) Rodriguez, V.; Aguirre-Zamlloa, G.; Couzi, M.; Roisnel, T. *J. Phys.: Condens. Matter.* **1996**, *8*, 969.
(20) Braud, M. N.; Couzi, M.; Chanh, N. B.; Courseille, C.; Gallois, B.; Hauw, C.; Meresse, A. *J. Phys.: Condens. Matter* **1990**, *2*, 8209.
(21) Samara, G. A.; Morosin, B.; Peercy, P. S. *Solid State Commun.* **1973**, *13*, 1525.
(22) Peercy, P. S.; Morosin, B.; Samara, G. A.; *Phys. Rev. B: Condes. Matter Mater. Phys.* **1973**, *8*, 3378.
(23) Kamenev, K.; Tancharakorn, S.; Robertson, N.; Harrison, A. *Rev. Sci. Instrum.*, in press.
(24) Murata, K.; Yoshino, H.; Yadav, H. O.; Honda, Y. *Rev. Sci. Instrum.* **1997**, *68*, 2490.
(25) Dingle, R.; Lines, M. E.; Holt, S. L. *Phys. Rev.* **1969**, *187*, 643.
(26) Specially prepared by Idemitsu Co., Ltd. Tokyo, Japan; it is registered as a manufacturing product with the name Daphne 7373.
(27) Merrill, L.; Bassett, W. A. *Rev. Sci. Instrum.* **1974**, *45*, 290.

Table 1. Crystallographic Data for TMMC at Increasing Pressures

pressure	0 kbar	2.1 kbar	3.8 kbar	6.8 kbar	12.2 kbar	17.0 kbar
chemical formula			$[(CH_3)_4N][MnCl_3]$			
Mr			235.44			
Z			2			
space group			hexagonal ($P6_3/m$)			
a (Å)	9.1880(13)	9.1287(3)	9.0893(4)	9.0215(6)	8.9326(2)	8.8728(8)
c (Å)	6.5230(13)	6.4903(5)	6.4724(7)	6.4395(10)	6.4010(4)	6.3620(14)
V (Å^3)	476.89(13)	468.40(4)	463.08(6)	453.88(8)	442.32(3)	433.76(11)
Mn−Cl distance (Å)	2.571(13)	2.565(11)	2.565(13)	2.554(15)	2.547(12)	2.536(3)
angle A (deg)[a]	78.72(5)	78.49(4)	78.37(5)	78.14(5)	77.84(4)	77.69(9)
angle B (deg)[a]	95.93(3)	95.76(3)	95.67(3)	95.50(4)	95.28(3)	95.17(7)
angle C (deg)[a]	84.07(3)	84.24(3)	84.33(3)	84.50(4)	84.72(3)	84.83(7)
R, wR_2, GOF	0.043,0.056,1.050	0.046,0.058,1.13	0.052,0.056,1.15	0.056,0.059,1.15	0.046,0.052,1.11	0.070,0.089,1.14

[a] Angles A, B, and C are defined in Figure 2.

the sample for subsequent pressure measurement using the ruby fluorescence technique. The gasket hole was flooded with a 4:1 methanol/ethanol mixture to act as a pressure-transmitting medium before the cell was finally assembled. X-ray diffraction data ($\lambda = 0.6984$ Å) were collected on a Bruker SMART diffractometer on Station 9.8 at CCLRC Daresbury Laboratory. Data were collected in ω-scans in 8 settings of 2θ and ϕ, following the strategy described by Dawson et al. (2004).[28] The data were integrated using the program SAINT[29] using "dynamic masks" to avoid integration over regions of the detector shaded by the body of the pressure cell.[28] Absorption corrections were carried out with the programs SADABS[30] and SHADE,[31] whereas merging was carried out in SORTAV[32] with robust-resistant weights. Data were collected on pressure increments up to 31 kbar, and the structures were refined between 0 and 17 kbar using the CRYSTALS code;[33] however, the raw data above this pressure were inadequate for either intensity integration or structure refinement due to degradation of the sample. This was manifested by the splitting of reflections. As the alignment of the splittings were directed along specific reciprocal lattice vectors, the degradation of the crystal is likely to be due to a structural phase transition. Refinement details and selected crystallographic parameters are shown in Table 1 and Figure 2. The R factor lies between 4 and 5% except for the 17 kbar data, for which the R factor was significantly worse (7%).

The crystal structure of TMMC adopts the $P6_3/m$ space group at conditions of ambient temperature and pressure, although it retains a strong $P6_3/mmc$ pseudosymmetry with the high-temperature parent phase (phase-I′). As the high-pressure experiments were conducted at ambient temperature, and we found no evidence of a phase transition until the sample started to form multiple domains at pressures greater than approximately 17 kbar, the structural refinements were performed assuming phase-I $P6_3/m$ symmetry. The Mn and N atoms were placed on the 2(b) (0,0,0) and 2(d) (1/3, 2/3, 1/4) special positions, respectively, whereas the Cl atom, 6(h) (x, y, 1/4), was initially located using the x and y coordinates reported by Braud et al.[20] at 293 K and allowed to vary during subsequent refinements. In previous structural studies of phase-I, the disordered tetrahedral $(CH_3)_4N$ counterion has been refined using a combination of two different models: model (1), where apical C atoms are disposed along the 3-fold axis and equatorial C atoms are placed above and below the mirror plane; and model (2), where alternate equatorial C atoms are placed on the mirror plane so that the apical C atoms occupy three sites around the 3-fold axis (see Figure 3 in Braud et al.[20]). For both of these models, the central N atom is fixed on the intersection between the mirror plane and 3-fold axis, and the tetrahedral shape of the molecule is retained in each of the disorder components. In the current study, the positions of the C atoms for the disordered $(CH_3)_4N$ counterion were determined from Fourier difference maps, and these were found to be consistent with model (1) of Braud et al.'s determination of the phase-I structure. We did not find sufficiently strong peaks in locations corresponding to model (2) to justify its inclusion in subsequent structural refinement of the high-pressure data. The ordered Mn, Cl, and N atoms could all be refined with anisotropic thermal displacement parameters, whereas those of the disordered C atoms were refined isotropically. The two symmetry inequivalent N−C bond lengths in model (1) were also restrained to have the same average distance in each refinement. As there are ambiguities regarding the positioning of the methyl hydrogen atoms, and with no clear evidence that they are ordered with regard to the C atom positions, the hydrogens were not included in the refinement.

Discussion

Structural Properties Under Pressure. The variation in structural parameters up to 17 kbar is shown in Table 1 and Figure 2. As expected from the effect of pressure, the distance between Mn atoms between chains has decreased from 9.188 to 8.873 Å over 17 kbar (3.4%). The distance between Mn atoms along the chain ((1/2)c) has also decreased from 3.261 to 3.181 Å over 17 kbar (about 2.5%), consistent with the expectation that the force between chains, Mn−$(CH_3)_4$N−Mn, is weaker than that along the chain, Mn−Cl_3−Mn. The lattice constants have been plotted as a function of pressure (Figure S1, Supporting Information). The axial compressibilities at room temperature in our case are $\kappa_a = -(\partial \ln a/\partial P)_T = 26 \times 10^{-4}$ kbar^{-1} and $\kappa_c = -(\partial \ln c/\partial P)_T = 18 \times 10^{-4}$ kbar^{-1}. The c/a ratio (Figure S2, Supporting Information) also shows that the Mn−Mn distance between chains decreases quicker than along the chain.

Magnetic Properties under Pressure. Due to the highly ideal, one-dimensional, Heisenberg-chain characteristics, the magnetic properties of TMMC have also been studied for many years. The long-range, three-dimensional antiferromagnetic ordering, as determined by both magnetic susceptibility[25] and specific heat capacity measurements,[34] does not occur until 0.84 K, indicating the very weak interaction between the magnetic chains. The short-range intrachain spin correlations lead to a broad maximum in the magnetic susceptibility at about 55 K (Figure 3).[35] Below this temperature, magnetic anisotropy can

(28) Dawson, A.; Allan, D. R.; Parsons, S.; Ruf, M. *J. Appl. Cryst.* **2004**, *37*, 410.
(29) Siemens, Area-Detector Integration Software, Siemens Industrial Autom., Madison, WI, 1995.
(30) Sheldrick G. M. University of Gottingen and Bruker AXS, Madison, WI, 2001.
(31) Parsons, S. *SHADE*. The University of Edinburgh, U.K., 2004.
(32) Blessing R. H. *J. Appl. Crystallogr.* **1997**, *30*, 421.
(33) Betteridge, P. W.; Carruthers, J. R.; Cooper, R. I.; Prout, K.; Watkin, D. J. *J. Appl. Cryst.* **2003**, *36*, 1487.
(34) de Jonge, W. J. M.; Swüste, C. H. W.; Kopinga, K.; Takeda, K. *Phys. Rev. B: Condes. Matter Mater. Phys.* **1975**, *12*, 5858.
(35) Walker, L. R.; Dietz, R. E.; Andres, K.; Darack, S. *Solid State Commun.* **1972**, *11*, 593.

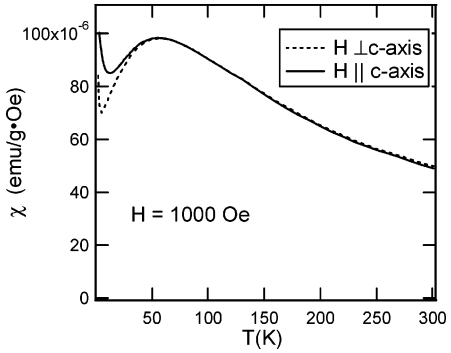

Figure 3. Magnetic susceptibility of TMMC showing the broad maximum at 55 K and magnetic anisotropy at lower temperature.

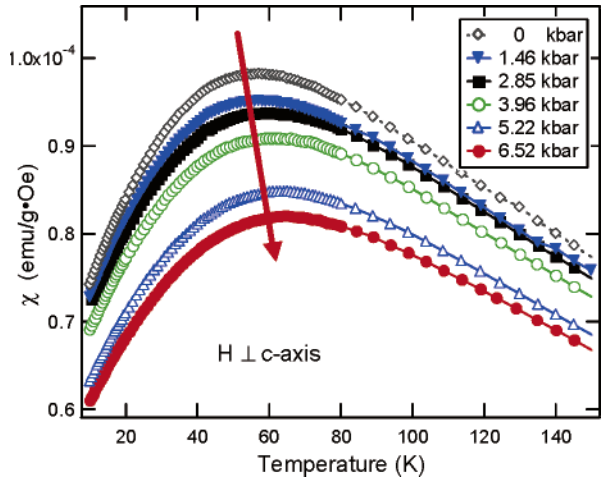

Figure 4. Temperature dependence of the broad maximum in the magnetic susceptibility of TMMC, T_{IAF}.

be observed due to preferred spin alignment perpendicular to the chain axis.

The effect of pressure on interchain interaction has been studied by magnetic heat capacity measurement and Raman scattering,[36] showing a change of the Néel temperature caused by pressure induction. However, the pressure effect on the short-range ordering of TMMC has not been studied previously, as this requires a very low background pressure cell. After removing the background, which is due to the material of the cell, our result shows that the peak moves toward higher temperature when the pressure increases (Figure 4).

The magnetic susceptibility of TMMC has been fit to the Fisher model[37] of the isotropic Heisenberg antiferromagnet for spin-$^1/_2$ system and later modified by Wagner and Friedberg[38] for Mn^{2+} system of spin $^5/_2$, which is

$$\chi_F = \frac{NS(S+1)}{3kT} g^2 \mu_B{}^2 \frac{1-u(K)}{1+u(K)} \qquad (1)$$

where $u(K)$ is $1/K - \coth(K)$, $K = 2JS(S+1)/kT$, $g = 2$, and $S = {}^5/_2$. J is negative for antiferromagnetic coupling. Due to the interaction between adjacent chains, the fit function can be modified to include the interchain coupling.[39] The function, therefore, is

$$\chi = \frac{\chi_F}{1 - (2zJ'/Ng^2\mu_B{}^2)\chi_F} \qquad (2)$$

where J' is the interchain exchange coupling constant and z is the number of the nearest neighbor chains.

Using this Fisher model with the molecular field correction, the diamagnetic correction, which is about 10^{-4} emu/mole, and avoiding the anisotropic interaction at low temperature, we obtained an excellent fit to the data from 40 to 300 K at all pressures (e.g., Figure 5), and the intrachain coupling constants for all pressures could therefore be obtained (Table 2). The pressure−temperature diagram (Figure 1, empty circles and inset) shows that the intrachain antiferromagnetic ordering temperature, T_{IAF}, has increased as a function of temperature. The slope (dotted line) has changed from 0.5 to 1.6 K/kbar at 2 kbar due to crossing the structural transition boundary (solid line). The model also gives the interchain coupling constant, which remained consistent at around −0.54 K at all pressures, which is very similar to previous work.[40,41] The low and invariant value is consistent with largely isolated chains.

In the magnetic susceptibility measurement, we have also observed small discontinuities in data at all pressures that correspond to the structural transition from the hexagonal to monoclinic phase (Figure 1, solid circles). The ambient pressure data show a small jump at 126 K, and the discontinuity point increases in temperature as the pressure increases. A similar phenomenon has also been observed in the magnetic susceptibility measurement of TMMBr at 145 K, the temperature at which the structural transition occurs.[42] We have extracted the transition temperatures from the $\Delta\chi/\Delta T$ against temperature (Figure 6) and observe an increase as a function of pressure.

The pressure−temperature phase diagram determined from these data (Figure 1) shows perfect agreement with Samara, Peercy, and Morosin's work.[22] The slope of transition temperature has changed from 5.2 to about 12 K/kbar at above 2 kbar. Consistent with the structural study, the results suggest the occurrence of a phase transition above 17 kbar, because extending the phase transition line toward room temperature suggests that, indeed, the phase transition could possibly occur around 17 kbar.

Relationship between Magnetic and Structural Data. Face-sharing octahedra of metal complexes represent a very common bridging motif in chain systems[14] and have also been studied as dinuclear species. Weighardt has reported a series of complexes of general formula $[LM^{II}(\mu\text{-}X)_3M^{II}L][BPh_4]$, where L = tridentate ligand, X = Cl, Br and M = Zn, Mn, Fe, Co, and Ni.[43] Comparison was also made to related systems that include V(II), other examples of the above metals, and related monoanionic bridging ligands. Comparison of the magnetic properties of the dinuclear species with the X-ray structures led to the conclusions that for d^3 metal ions (e.g., V(II), Cr(III), and Mn(IV)) magnetic exchange occurs through direct interaction of the magnetic orbitals that are directed between the ligands (t_{2g} in octahedral symmetry). For these, J was correlated with

(36) Takeda, K.; Suzuki, T. *Jpn. J. App. Phys.* **1987**, *26*, 859.
(37) Fisher, M. E. *Am. J. Phys.* **1963**, *32*, 343.
(38) Wagner, G. R.; Friedberg, S. A.; *Phys. Lett.* **1964**, *9*, 11.
(39) McElearney, J. N.; Merchant, S.; Carlin, R. L. *Inorg. Chem.* **1973**, *12*, 906.
(40) Caputo, R. E.; Willet, R. D. *Phys. Rev. B: Condes. Matter Mater. Phys.* **1976**, *9*, 3956.
(41) Gaulin, B. D.; Collins, M. F. *Phys. Rev. B: Condes. Matter Mater. Phys.* **1986**, *33*, 6287.
(42) Tanaka, H.; Tsuruoka, F.; Ishii, T.; Izumi, H.; Iio, K.; Nagata, K. *J. Phys. Soc. Jpn.* **1986**, *55*, 2369.
(43) Bossek, U.; Nuhlen, D.; Bill, E.; Glaser, T.; Krebs, G.; Weyhermuller, T.; Wieghardt, K.; Lengen M.; Trautwein, A. X. *Inorg. Chem.* **1997**, *36*, 2834.

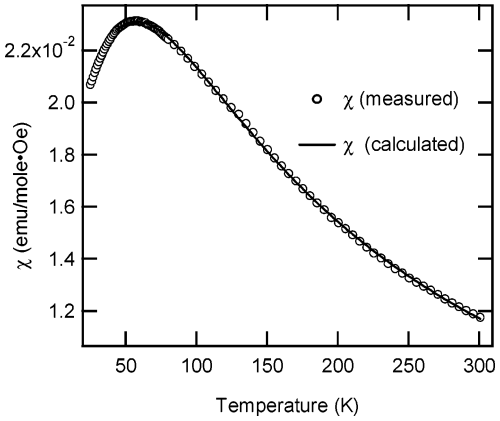

Figure 5. Magnetic susceptibility of TMMC at 0 kbar showing best fit with the corrected Fisher model.

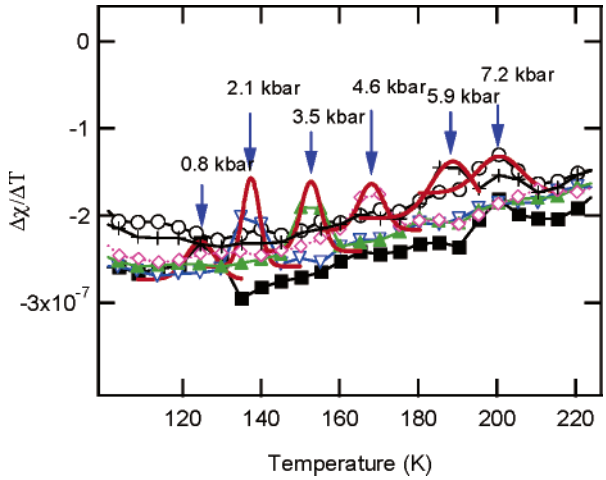

Figure 6. The temperature dependence of $\Delta\chi/\Delta T$ at various pressures showing the peaks corresponding to the hexagonal to monoclinic structural transition temperatures.

Table 2. Intrachain Antiferromagnetic Ordering Temperature (T_{IAF}) and J/k

pressure (kbar)	T_{IAF} (K)	J/k (K)
0.0	57.2	−6.85
0.3	57.3	−6.91
1.5	58.0	−6.96
2.9	59.7	−7.21
4.0	61.8	−7.38
5.2	64.0	−7.66
6.5	64.6	−7.81

the M−M distance and was essentially independent of the nature and geometry of the bridging ligands. In contrast, for a metal such as Ni(II), d^8, the magnetic orbitals will be directed toward the ligands, and accordingly, such species show no correlation between J and the M−M distance. Instead, distances, angles, and ligands involved in the bridging interaction play a crucial role in mediating the superexchange. For a high-spin d^5 metal such as the Mn(II) system studied in this work, the situation may clearly be more complicated, with the possibility of contributions from both direct exchange and superexchange in the magnetic coupling. This is illustrated by the study of Mn(II) dimers bridged by two azide ligands, where the ferromagnetic coupling was attributed to the geometry of the superexchange interaction.[1] In this case, however the Mn···Mn separation was considerably larger than in this work (3.478−3.537 Å compared with 3.181−3.262 Å) such that the contribution of direct exchange between Mn d orbitals may be much less significant in comparison with our study (see below).

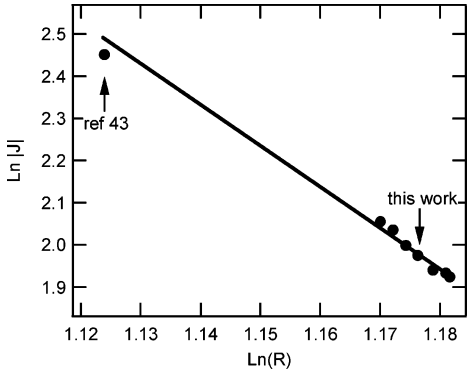

Figure 7. Ln(−J) as a function of ln(R) showing the linearity of our results and comparison with the binuclear complex of Wieghardt.[43]

Analysis of bond lengths and angles within the structure of TMMC as pressure is varied reveals significant changes. As would be expected from compression along the chain direction, angles A and B become narrower and angle C becomes wider (Figure 2, Table 1). In addition, the Mn−Cl bond distance drops by over 1%. The largest angular change, of around 1.6%, occurs in the Mn−Cl−Mn angle A, which is narrowed from 78.75 to 77.48°, further from the 90° angle that would be expected to give a maximum in ferromagnetic superexchange.[2,3] Thus, the angular changes in the system are consistent with an increase in antiferromagnetic coupling, as is observed.

As would be expected, we also observed changes in distances between Mn atoms along the chain. According to the relationship developed by Bloch,[12] we plotted ln(−J) against ln(R) (where R = Mn−Mn distance along the chain), and this yielded a straight-line plot with a slope of approximately −10 in keeping with the general empirical relationship. We compared this graph to the exchange coupling constant and the Mn−Mn interaction in the binuclear complex of Weighardt $[L_2Mn_2(\mu\text{-}Cl)_3]BPh_4$, where L is 1,4,7-trimethyl-1,4,7-triazacyclononane and Ph is phenyl.[43] Strikingly, we observe that despite the large differences in both J and the Mn−Mn distance between the binuclear complex and the TMMC chain, the binuclear complex lies very close to the same linear relation (Figure 7). Initial inspection of these results would suggest that a direct exchange mechanism dominates the coupling within the triply bridged $Mn(\mu\text{-}Cl)_3Mn$ system because the exchange coupling appears to correlate with the Mn−Mn distance as a sole parameter. Some caution should be exercised however, because the general trend of the superexchange contribution to the coupling will also be toward a stronger antiferromagnetic interaction as the chain is compressed and angle A is narrowed. Thus, the correlation of J with the Mn−Mn distance may prove an empirical predictor of J without necessarily revealing the orbital origins of the coupling mechanism in detail. Further work on d^3, d^5, and d^8 chain systems is planned to explore the relative contributions of superexchange and direct exchange in such materials.

Conclusions

We have carried out a systematic study of the magnetic properties and single-crystal X-ray structure of TMMC at various pressures in a novel approach toward the build up of structure−property relationships in a rapid, facile manner.

Analysis of the data suggests a correlation between the Mn−Mn intrachain distance and the intrachain coupling constant J, consistent with the relationship derived by Bloch for simple insulators. This may suggest that the interaction is dominated by direct exchange between the metal orbitals (t_{2g} in octahedral symmetry), although further work is planned to build more-detailed structure−property comparisons in these and related transition-metal systems.

One potential limitation of our current approach concerns the comparison of structural data taken at ambient pressure with magnetic data derived from a fit over a broad temperature range. In further theoretical work, detailed calculation of magnetic properties based on structural parameters may be limited unless simultaneous low-temperature, high-pressure studies become experimentally more accessible; however, for the development of empirical correlations, any effects of temperature will be simply incorporated into the correlation obtained. Furthermore, according to Peercy, Morosin, and Samara, less than a 1% change of the c axis of TMMC occurs over 200 K,[22] suggesting that any temperature effects are less than the changes induced by application of moderate pressures.

We chose to study a system that includes large organic counterions and, although this successfully led to effective separation of the magnetic chains at all pressures, the associated disorder is also responsible for the varied phases displayed by the system. At room temperature, the space group of TMMC is $P6_3/m$, as reflected in the structural data up to 17 kbar, whereas the magnetic data revealed the presence of the additional two monoclinic phases. Although such rich phase behavior is an important topic in its own right, for the development of structure−property correlations in magnetic materials, it can lead to additional complication. We note, however, that all the phases retain well-separated magnetic chains with Mn(II) ions lying along the c axis, allowing meaningful comparison of data over the full temperature and pressure range. The correlation of structural and magnetic data achieved here suggests that similar systems are appropriate for future work, although we will also explore the use of lower-symmetry organic counterions to simplify the $P-T$ phase diagram.

Acknowledgment. We thank The Royal Thai Government for a studentship (S.T.), Daresbury Laboratory SRS, and Dr. John Warren for assistance with the synchrotron radiation experiments.

Supporting Information Available: Crystallographic data at each pressure in Table 1 (CIF format), Figures S1 and S2. This material is available free of charge via the Internet at http://pubs.acs.org.

JA061923I